Commun Nonlinear Sci Numer Simulat 18 (2013) 2916–2925

Contents lists available at SciVerse ScienceDirect

Commun Nonlinear Sci Numer Simulat

journal homepage: www.elsevier.com/locate/cnsns

Effect of contact stiffness modulation in contact-mode AFM under subharmonic excitation

Ilham Kirrou, Mohamed Belhaq *

Laboratory of Mechanics, University Hassan II-Casablanca, Morocco

ARTICLE INFO

Article history:
Received 10 August 2012
Received in revised form 6 February 2013
Accepted 6 February 2013
Available online 24 February 2013

Keywords:
Atomic force microscopy
Subharmonic response
Contact stiffness modulation
Frequency shift
Perturbation method

ABSTRACT

We report on the effect of fast contact stiffness modulation on frequency response to 2:1 subharmonic resonance in contact-mode atomic force microscopy. The model of the contact-mode dynamic between the tip of the microbeam and the moving surface consists of a lumped single degree of freedom Hertzian contact oscillator. Perturbation methods are applied to obtain the frequency response of the slow dynamic of the system. We focus on the effect of the amplitude and the frequency of the modulation on the nonlinear characteristic of the contact stiffness, the jump phenomenon and the shift in the frequency response of the subharmonic. We also show the effect of the contact stiffness modulation on the interval of the unstable trivial solution which is directly correlated to the depth of the jump. The obtained results can directly influence the material properties and the loss of contact between the tip and the sample.

1. Introduction

In contact-mode atomic force microscopy (AFM) [1] the surface force can be confined to a Hertzian contact regime between the tip of the micro-scale cantilever and the moving surface. The performance of such a contact-mode AFM in imaging the surface requires the contact-mode regime to be maintained during the scan. However, it is known that for a slight increase of the amplitude of the sample surface driving, contact losses may occur near resonances causing impacts, thereby a possible deterioration of the device [2,3]. Based on numerical simulations, analytical approximation and experimental results [3,4], it was concluded that the loss of contact is generally initiated by jump of amplitude near resonances. The loss of contact can also be triggered when the amplitude of the response is hight. Hence, controlling the response amplitude and the location where jumps occur is of great importance, in the sense of manipulation and imaging performance of surfaces.

The control of the location of jumps in macro-scale forced impacting Hertzian contact oscillators has been investigated recently and some strategies were proposed [5,6]. The first strategy introduced a fast harmonic excitation added from above to the basic forcing, the second one used a fast harmonic base displacement, while the third one introduced a fast harmonic parametric stiffness. It was concluded that the harmonic base displacement shifts the frequency response left, whereas the parametric stiffness shifts it right. While the effect of fast excitations on macro-scale systems has been studied in various applications [7,8,5,6,9,10], it has received little attention only in micro-scale devices [11,12].

In the absence of contact stiffness modulation, Turner [13] investigated the nonlinear vibrations of a linear beam with cantilever Hertzian contact boundary conditions assuming that the beam remains in contact with the moving surface. He used the method of multiple scales (MMS) [14,15] to approximate the response of the probe-tip sample system to primary

* Corresponding author.
E-mail address: mbelhaq@yahoo.fr (M. Belhaq).

1007-5704/$ - see front matter © 2013 Elsevier B.V. All rights reserved.
http://dx.doi.org/10.1016/j.cnsns.2013.02.008

resonance excitation. It was observed that the response of the first mode is more willing to loose contact near the resonance before a significant change of parameters.

In a recent work [16], preliminary results for a single degree of freedom (SDOF) reported the effect of fast contact stiffness modulation on the frequency response in a contact-mode AFM near primary resonance. Hysteresis was observed which results in transition behavior between two stable oscillation regimes of the microcantiliver. This bistability is, in fact, correlated to instabilities in scanning operation. It was concluded that fast contact stiffness modulation can eliminate such a bistability in a certain range of the modulation amplitude allowing the contact-mode AFM to be maintained.

In the present work, we report on the effect of fast contact stiffness modulation on the frequency response to 2:1 subharmonic resonance. This study is motivated by the fact that excitation of subharmonics in AFM can be a promising technique in imaging surfaces with high spatial resolution [17–19]. Moreover, subharmonic contact resonance regimes not only was observed in dynamic AFM [20] but also it can be exploited in contact-mode AFM to estimate the nonlinear coefficients of the contact stiffness [21]. More interestingly, recent works reported that excitation of subharmonics holds interesting physical insights [17–19] and thus modeling and exploring the dynamic of the tip and the sample in different interaction regimes will help shedding light on the physical mechanism exciting subharmonics in AFM in general and in the amplitude modulation AFM mode of operation, in particular. Notice that the response near the subharmonic resonance is different from that of primary resonance. Unlike the case of primary resonance, the response of the subharmonic experiences a sharp jump from small response to large one as the frequency is swept passing resonance. Further, there is no hysteresis near the subharmonic resonance.

Since the first mode of the microbeam is predisposed to lose contact with a slight change of parameters [13], a SDOF Hertzian contact oscillator modeling the first mode cantilever dynamics of contact-mode AFM is considered. Although the response of AFM cantilever is highly nonlinear and difficult to explore, a SDOF model is often adopted to model the first mode cantilever neglecting the higher-order flexural modes. Indeed, a SDOF is considered as a good model to approximate real phenomenon in ambient conditions [17] since the dominant eigenmode is sufficient to describe the cantilever's dynamic motion [22].

In the next Section we present the equation of motion under Hertzian contact condition with a contact stiffness modulation. The method of direct partition of motion (DPM) is applied to obtain the main equation of motion describing the slow dynamic of the tip-sample system. In Section 3, the MMS is implemented on the slow dynamic to derive the amplitude-phase modulation equations for the subharmonic resonance and to study the effect of contact stiffness modulation on the nonlinear contact resonance. Section 4 concludes the work.

2. Equation of motion and slow dynamic

The lumped parameter SDOF contact-mode AFM model with fast contact stiffness modulation, as shown in Fig. 1 [23], is studied. The equation of motion of the system is given by

$$m\ddot{x} + c_1\dot{x} + kx = -(k_0 + k_1\cos\Omega_2 t)(z_0 - x)^{\frac{3}{2}} + mg + F\cos\Omega_1 t \tag{1}$$

Here x is the effective displacement of the cantilever tip, m is the lumped cantilever mass, c_1 $(= c_0 + c_*)$ the effective damping constant, k the free cantilever stiffness, k_0 the constant given by the Hertzian theory [24] which is associated with the radius, AFM tip and substrate moduli and Poisson' s ratios, k_1, Ω_2 the amplitude and the frequency of the fast contact stiffness modulation, z_0 the surface offset, g the acceleration gravity, and F, Ω_1 are, respectively, the amplitude and the frequency of the sample vibration [25,26]. The displacement x is defined by considering the static problem as $x = x_s + X$ and the quantity $\Delta = z_0 - x_s$ as the static Hertz deformation, where x_s is the static position and X is the displacement from the static position.

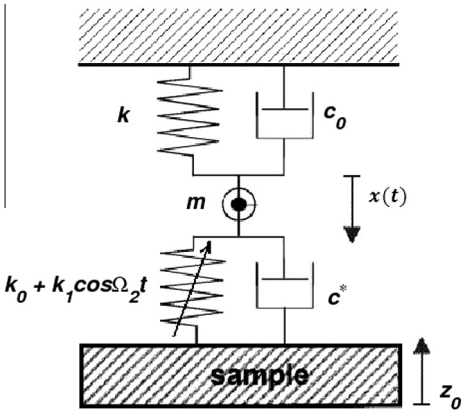

Fig. 1. A shematic of SDOF model of a tip-sample AFM (from [23]).

From application view point, the contact stiffness modulation can be introduced in contact-mode AFM by excited the cantilever using ultrasonic transducer attached to the cantilever [27] and increasing the amplitude of the z-piezo or by increasing the amplitude in the transducer bounded underneath the sample as in the atomic force acoustic microscopy [26,28,29].

Introducing the variable changes as $u=\frac{X}{\Delta}$, $\tau=\omega_0 t, \omega_0^2=\frac{k}{m}$, $c=\frac{c_1}{m\omega_0}$, $\beta=\frac{3k_0\Delta^2}{2m\omega_0^2}$, $\beta_1=\frac{\beta}{4}, \beta_2=\frac{\beta}{24}$, $f=\frac{F}{m\omega_0^2\Delta}, \omega=\frac{\Omega_1}{\omega_0}$ and $\Omega=\frac{\Omega_2}{\omega_0}$, the dimensionless equation of motion takes the form

$$\ddot{u}+c\dot{u}+u-\frac{2}{3}\beta+\frac{2}{3}\beta(1+r\cos\Omega\tau)(1-u)^{\frac{3}{2}}=f\cos\omega\tau \tag{2}$$

where $\dot{(\ )}=\frac{d}{d\tau}$ and $r=\frac{k_1}{k_0}$ is the ratio between the modulated and the unmodulated contact stiffness coefficients.

Expanding the nonlinear restoring force in Taylor series around the static load and keeping only terms up to order three in u, Eq. (2) reads

$$\ddot{u}+\varpi^2u+c\dot{u}+\beta_1u^2+\beta_2u^3+r\left(\frac{3}{2}\beta-\beta u+\beta_1u^2+\beta_2u^3\right)\cos\Omega\tau=f\cos\omega\tau \tag{3}$$

where $\varpi=\sqrt{1-\beta}$ is the natural frequency with the condition $\beta<1$ to be satisfied. Eq. (3) contains a slow dynamic due to the external excitation of the sample and a fast dynamic produced by the frequency of the contact stiffness modulation, Ω, supposed large with respect to the frequencies ϖ and ω. In this case, the method of DPM [7,8] can be performed to study the effect of fast contact stiffness modulation on the frequency response of the system.

Introducing two different time scales, a fast time $T_0=\Omega\tau$ and a slow time $T_1=\tau$, and splitting up $u(\tau)$ into a slow part $z(T_1)$ and a fast part $\psi(T_0,T_1)$ as

$$u(\tau)=z(T_1)+\psi(T_0,T_1) \tag{4}$$

where z contains a slow dynamic which describes the main motions at time-scale of the tip natural vibrations and ψ stands for an overlay of the fast motions at time scale of the parametric excitation. The fast part ψ and its derivatives are assumed to be 2π–periodic functions of fast time T_0 with zero mean value with respect to this time, so that $\langle u(t)\rangle=z(T_1)$ where $\langle\rangle\equiv\frac{1}{2\pi}\int_0^{2\pi}()\,dT_0$ defines time-averaging operator over one period of the fast excitation with the slow time T_1 fixed. Introducing $D_i^j\equiv\frac{\partial^j}{\partial^j T_i}$ yields $\frac{d}{dt}=\Omega D_0+D_1$, $\frac{d^2}{dt^2}=\Omega^2D_0^2+2\Omega D_0D_1+D_1^2$ and substituting Eq. (4) into Eq. (3) gives

$$\begin{aligned}&\ddot{z}+\ddot{\psi}+c(\dot{z}+\dot{\psi})+\varpi^2(z+\psi)+\beta_1(z+\psi)^2+\beta_2(z+\psi)^3+\frac{3}{2}r\beta\cos\Omega\tau-r\beta(z+\psi)\cos\Omega\tau+r\beta_1(z+\psi)^2\cos\Omega\tau\\&\quad+r\beta_2(z+\psi)^3\cos\Omega\tau=f\cos\omega\tau\end{aligned} \tag{5}$$

Averaging (5) leads to the main equation governing the slow dynamic of the motion

$$\ddot{z}+\omega_1^2z+c\dot{z}+\rho_1z^2+\rho_2z^3+H=f\cos\omega\tau \tag{6}$$

Details of the calculation to derive Eq. (6) as well as the expressions of parameters $\omega_1^2, \rho_1, \rho_2$ and H are give in the Appendix.

Fig. 2 shows a comparison between the full motion $u(\tau)$, (3), and the slow dynamic $z(\tau)$, (6), for the given parameters $c=0.05, f=0.008, \beta=0.8, \Omega=3$, $\sigma=0.01$ and $r=0.2$, thereby validating the DPM method.

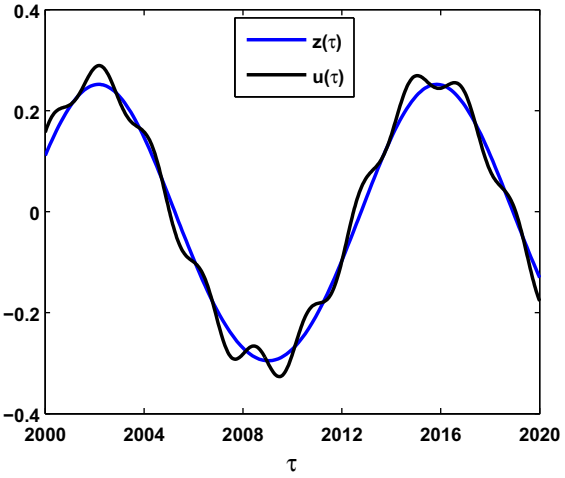

Fig. 2. Comparison between the full motion, (3), and the slow dynamic, (6).

3. Frequency response analysis near 2:1 resonance

In this Section we investigate the frequency–response curve of the slow dynamic (6) applying the MMS [14,15] near the 2:1 resonance condition and we examine the effect of the contact stiffness modulation on the frequency response.

To approximate the frequency response near the 2:1 resonance, we express the resonance condition by introducing a detuning parameter σ according to

$$\omega = 2\omega_1 + \sigma \tag{7}$$

Introducing a bookkeeping parameter ϵ and scaling as $f = \epsilon f, \rho_1 = \epsilon\rho_1$, $\rho_2 = \epsilon^2\rho_2, c = \varepsilon^2 c$ and $H = \epsilon H$, Eq. (6) can be rearranged in the form

$$\ddot{z} + \omega_1^2 z = -\epsilon(\rho_1 z^2 + H - f\cos\omega\tau) - \epsilon^2(c\dot{z} + \rho_2 z^3) \tag{8}$$

Steady-state solution are expanded as

$$z(T_0, T_1, T_2) = z_0(T_0, T_1, T_2) + \epsilon z_1(T_0, T_1, T_2) + \epsilon^2 z_2(T_0, T_1, T_2) + 0(\epsilon^3) \tag{9}$$

where $T_0 = \tau, T_1 = \epsilon\tau$ and $T_2 = \epsilon^2\tau$. In terms of the variables $T_i (i = 0, 1, 2)$, the time derivatives become $\frac{d}{d\tau} = D_0 + \epsilon D_1 + \epsilon^2 D_2 + O(\epsilon^3)$ and $\frac{d^2}{d\tau^2} = D_0^2 + 2\epsilon D_{01} + \epsilon^2 D_1^2 + 2\epsilon^2 D_{02} + O(\epsilon^3)$, where $D_i = \frac{\partial}{\partial T_i}$. Substituting (9) into (8) and equating the terms with the same order of ϵ, yields

$$D_0^2 z_0 + \omega_1^2 z_0 = 0 \tag{10}$$

$$D_0^2 z_1 + \omega_1^2 z_1 = -2D_0 D_1 z_0 - \rho_1 z_0^2 - H + f\cos(\omega\tau) \tag{11}$$

$$D_0^2 z_2 + \omega_1^2 z_2 = -2D_0 D_1 z_1 - (D_1^2 + 2D_0 D_2) z_0 - cD_0 z_0 - 2\rho_1 z_0 z_1 - \rho_2 z_0^3 \tag{12}$$

The solution of Eq. (10) is assumed to be in the form

$$z_0(T_0, T_1) = A(T_1)e^{i\omega_1 T_0} + cc \tag{13}$$

where $A(T_1)$ is a complex amplitude and *cc* stands for the complex conjugate of the preceding term. Substituting Eqs. (7) and (13) into (11), (12) and removing secular terms, we obtain

$$\rho_{en} A^2 \bar{A} + \rho_{el} A + i(-2\omega_1 D_2 A - c\omega_1 A) - \rho_{ef}\bar{A}e^{i\sigma T_2} = 0 \tag{14}$$

where

$$\rho_{en} = \frac{10\rho_1^2}{3\omega_1^2} - 3\rho_2 \tag{15}$$

$$\rho_{ef} = \frac{\rho_1 f}{\omega_1^2 - (2\omega_1 + \sigma)^2} \tag{16}$$

Here ρ_{en} and ρ_{ef} are the effective nonlinear and the effective forcing coefficients, respectively, and $\rho_{el} = \frac{2\rho_1 H}{\omega_1^2}$ is the linear coefficient. Eq. (14) can be solved for the complex amplitude by introducing its polar form as

$$A = \frac{1}{2} a e^{i\theta} \tag{17}$$

Thus, the modulation equations of amplitude and phase can be extracted as

$$\begin{cases} \frac{da}{dt} = -\frac{1}{2}ca - \frac{\rho_{ef}}{2\omega_1} a\sin\varphi \\ a\frac{d\varphi}{dt} = (\sigma + \frac{\rho_{el}}{\omega_1})a + \frac{\rho_{en}}{4\omega_1}a^3 - \frac{\rho_{ef}}{\omega_1}a\cos\varphi \end{cases} \tag{18}$$

in which $\varphi = \sigma T_2 - 2\theta$. Periodic solutions of Eq. (8) correspond to stationary solutions of the modulation equations (18), i.e. $\dot{a} = \dot{\varphi} = 0$. These stationary solutions are given by the following algebraic equation

$$a^2\left[\left(\sigma + \frac{\rho_{el}}{\omega_1} + \frac{\rho_{en}}{4\omega_1}a^2\right)^2 + c^2\right] = \left(\frac{\rho_{ef}}{\omega}\right)^2 a^2 \tag{19}$$

Eq. (19) has a trivial solution ($a = 0$) and nontrivial ones given by

$$a^2 = \frac{4\omega_1}{\rho_{en}}\left[\left(\sigma + \frac{\rho_{el}}{\omega_1}\right) \pm \sqrt{c^2 + \left(\frac{\rho_{ef}}{\omega_1}\right)^2}\right] \tag{20}$$

In frequency sweep (i.e., for a given effective forcing ρ_{ef}), the critical detuning parameter σ_c given by

$$\sigma_c = -\frac{\rho_{el}}{\omega_1} \pm \sqrt{c^2 + \left(\frac{\rho_{ef}}{\omega_1}\right)^2} \tag{21}$$

defines an interval $[-\sigma_c, \sigma_c]$ of forcing frequencies within which the trivial solution is unstable.

In a force sweep (i.e., for a given detuning σ), the critical forcing level

$$F_c = \left| \left(\frac{\omega_1^3 - \omega_1(2\omega_1 + \sigma)^2}{\rho_1} \right) \sqrt{\left(\sigma + \frac{\rho_{el}}{\omega_1}\right)^2 - c^2} \right| \tag{22}$$

defines a threshold above which the trivial solution is always unstable.

3.1. Case without contact stiffness modulation ($r = 0$)

In the absence of the modulation, the main results are reported in Figs. 3 and 4. Figure 3 shows the variation of the frequency response, as given by Eq. (19), for fixed c and β and for two values of the amplitude of the external excitation f. The nonlinear softening behavior characterized by a decrease in frequency with amplitude is obtained. This type of behavior has been reported for primary resonance as well [16]. The solid lines denote stable solutions, the dashed lines denote unstable ones and results obtained from direct numerical simulation of Eq. (6) (circles) using Runge–Kutta method are plotted for validation. This figure shows that increasing the amplitude of the excitation f, the instability interval of the trivial solution increases.

Fig. 4 illustrates the frequency response for different values of the contact stiffness β in the absence of the modulation. The curves show that increasing β softens the system, decreases the amplitude of the response and increases the instability interval of the trivial solution. Note that the instability interval of the trivial solution is correlated to the jump depth of the response from the trivial to nontrivial stable solution. The increase of the softening behavior and the amplitude of the response have also been observed for primary resonance [16].

3.2. Case with contact stiffness modulation

Next, we consider the case where the contact stiffness modulation is present ($r \neq 0$). The effect of the frequency of this modulation Ω on the frequency response is illustrated in Fig. 5 showing that an increase of Ω softens the system, shifts the subharmonic resonance toward lower frequencies and increases the interval of the unstable trivial solution.

Fig. 6 shows the changes of the shift direction in the frequency–response curves for fixed Ω and for increasing values of the amplitude of the contact stiffness modulation r. It can be seen in Fig. 6a that the resonance curve undergoes a significant shift toward higher frequencies while the interval $[\sigma_{cl}, \sigma_{cr}]$ of the unstable trivial solution decreases. Increasing the amplitude r further, the frequency response continues shifting right until reaching a some critical value (Fig. 6b, $r \approx 0.7$). Beyond this value the resonance curve changes the shift direction toward lower frequencies (Fig. 6b for $r = 0.9$ and $r = 1$) and the instability interval of the trivial solution continues to decrease causing the jump depth of the response to reduce. This means that driving the cantilever with relatively large amplitude of contact stiffness modulation may reduce the jump depth.

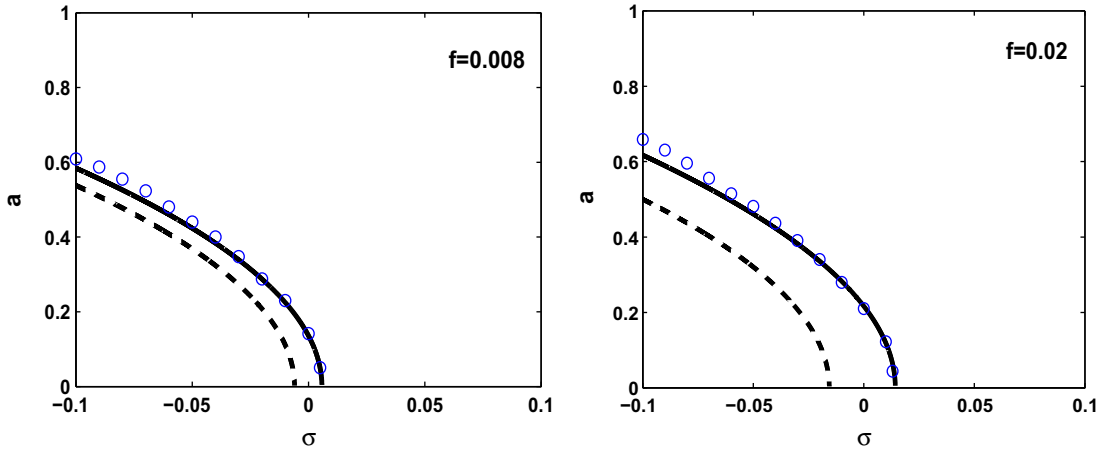

Fig. 3. Frequency–response curves for $c = 0.001, \beta = 0.8$ and for different values of f.

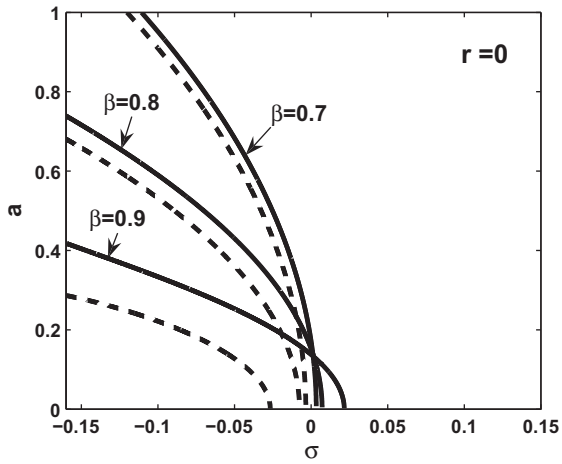

Fig. 4. Frequency–response curves for $f = 0.01, c = 0.001$ and for different values of β.

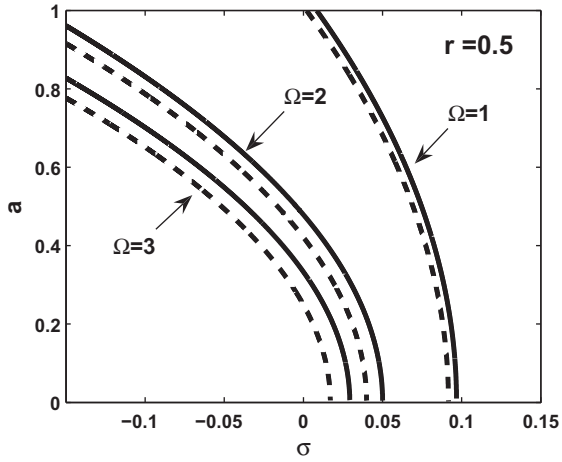

Fig. 5. Frequency–response curves for $r = 0.5, c = 0.001, f = 0.01, \beta = 0.8$ and for different values of Ω.

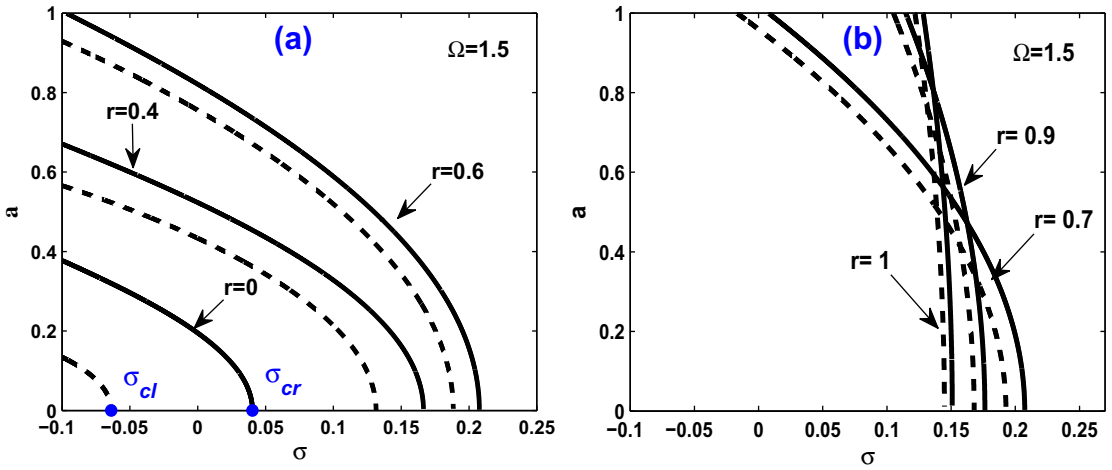

Fig. 6. Frequency–response curves for $\beta = 0.9, c = 0.001, f = 0.02$ and for different values of r.

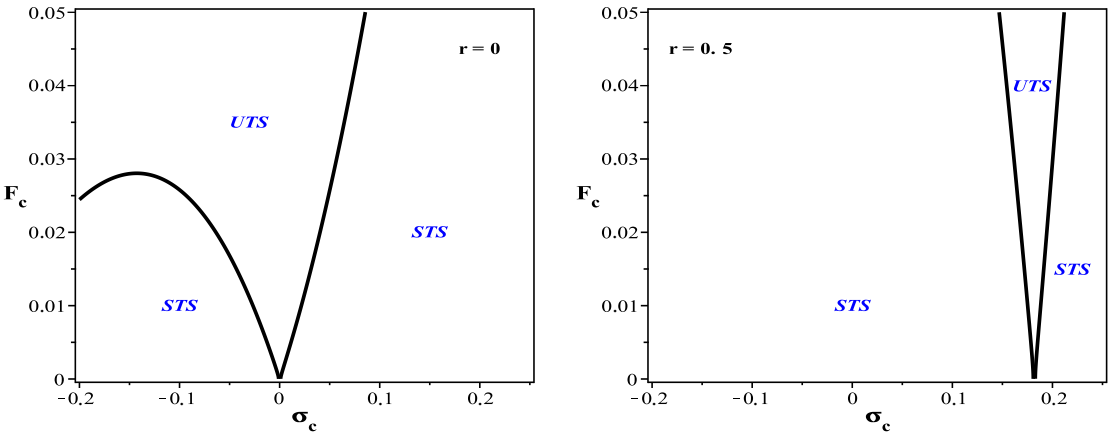

Fig. 7. Variation of the critical forcing F_c with σ_c for $c = 0.001, \beta = 0.9$ and $\Omega = 1.5$ (STS: stable trivial solution and UTS: unstable trivial solution).

In Fig. 7 we plot in the parameter plane, the critical forcing F_c versus the critical detuning σ_c, the curves given by the condition (22). These curves separate the regions where the system oscillates either at the forcing frequency ω (i.e., $a = 0$: stable trivial solution region (STS)), or at the subharmonic resonance frequency which is activated when crossing the curves (i.e., $a \neq 0$: unstable trivial solution region (UTS)). It can be seen that for increasing r, the domain of unstable trivial solution decreases significantly and shifts toward higher frequencies. This indicates that the amplitude of the contact stiffness modulation strongly influence the location as well as the interval of unstable trivial solution, which is directly related to jump phenomenon from the trivial to nontrivial stable branch of subharmonic solution.

Fig. 8 shows in the parameter plane, critical detuning σ_{cl}, σ_{cr} versus r, the variation of the interval $[\sigma_{cl}, \sigma_{cr}]$ of unstable trivial solution, as given by Eq. (21). This figure indicates that as r increases, this interval decreases, shifts toward higher frequencies until r reaching a certain critical value and then shifts back toward lower frequencies. Note also the decreasing of the interval of unstable trivial solution with increasing r.

In Fig. 9 we show in the parameter plane (r, Ω) the curve $\rho_{en} = 0$ given by Eq. (15) separating the domains of softening and hardening behaviors, and the curve $\sigma_{cmax} = 0$ given by Eq. (21) corresponding to the location where the shift of the frequency response changes direction. Three regions can be distinguished in this figure. When increasing r, in region I the frequency response has a softening behavior and shifts to the right (see Fig. 10a for $r = 0.6$), in region II the frequency response changes its direction and shifts back toward lower frequencies (see Fig. 10a for $r = 0.8$), whereas in region III, the frequency response continues shifting left and the hardening behavior appears (see Fig. 10b for $r = 1$). Fig. 10 illustrates these effects on the frequency response. The solid lines and the dashed lines denote analytical solution while the circles denote numerical simulation using Runge–Kutta method. The comparison between the analytical result and the numerical simulation confirms the observed effects.

It is worth noticing that based on the obtained results, the change of the shift direction is generated by the presence of the quadratic nonlinearity in the model.

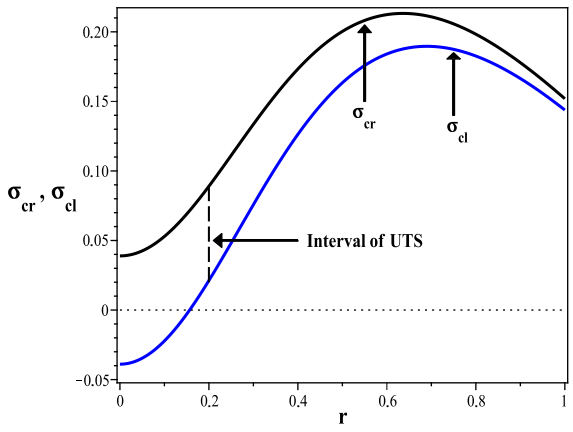

Fig. 8. Variation of the interval of unstable trivial solution with r for $f = 0.02, c = 0.001, \beta = 0.9, \sigma = 0.05$ and $\Omega = 1.5$. Subscribe (cl): critical left; subscribe (cr):critical right.

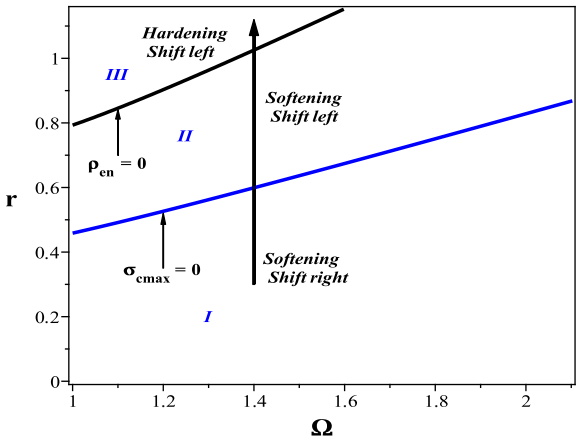

Fig. 9. Curve separating the three regions I, II and III in the plan (Ω, r) for $c = 0.001, \beta = 0.9$ and $f = 0.02$.

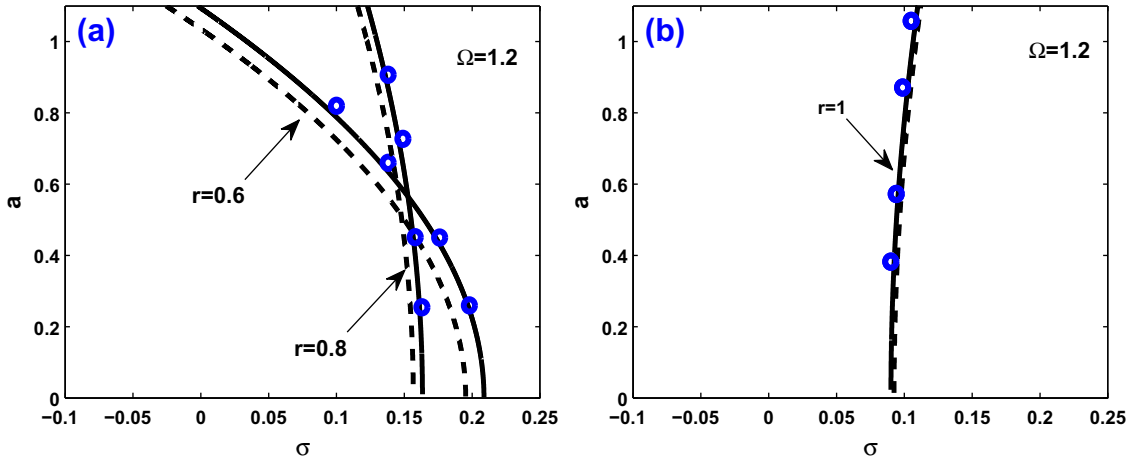

Fig. 10. Frequency–response curves for $\beta = 0.9, c = 0.001, f = 0.02$ and for different values of r.

4. Conclusions

This paper studies the effect of a fast contact stiffness modulation on the 2:1 subharmonic response of a contact-mode AFM modeled by a lumped SDOF Hertzian contact oscillator. The technique of DPM coupled with the MMS was performed to determine the frequency response of the slow dynamic to the subharmonic resonance. We have shown that the amplitude and the frequency of the contact stiffness modulation strongly influence the characteristic of the nonlinear contact stiffness as well as the location and the length of the interval of unstable trivial solution. Specifically, increasing the amplitude of the contact stiffness modulation leads the response curve to shifts toward higher frequencies until reaching a critical position and then shifts back toward lower frequencies. On the other hand, the increase of the modulation amplitude causes the amplitude of oscillation to increase reflecting a stiffer contact between the tip and the sample. Also, an increase of the modulation amplitude decreases drastically the length of the interval of the unstable trivial solution resulting in reducing the jump depth, thereby the possibility of the contact loss to trigger.

More clearly, it can be concluded that the contact stiffness characteristic of the sample, the shift in the contact resonance frequency and the interval of the unstable trivial solution can be controlled by monitoring the contact stiffness modulation parameters.

The the results of the present work shown that investigation of subharmonics in contact-mode AFM can be a promising issue in imaging surfaces with high performance, and therefore, the analysis of subharmonics is of significant interest and likely can help shedding light on the physical mechanism induced when subharmonics are activated in different interaction regimes of AFM.

Appendix A

Averaging Eq. (5) leads to

$$\ddot{z} + c\dot{z} + \varpi^2 z + \beta_1 z^2 + \beta_1\langle\psi^2\rangle + \beta_2 z^3 + 3\beta_2 z\langle\psi^2\rangle + \beta_2\langle\psi^3\rangle + r[-\beta\langle\psi\rangle + 2\beta_1 z\langle\psi\rangle + \beta_1\langle\psi^2\rangle + 3\beta_2 z^2\langle\psi\rangle + 3\beta_2 z\langle\psi^2\rangle + \beta_2\langle\psi^3\rangle]\cos\Omega\tau = f\cos\omega\tau \tag{23}$$

and subtracting (23) from (5) yields

$$\ddot{\psi} + \psi + 2\beta_1 z\psi + \beta_1\psi^2 - \beta_1\langle\psi^2\rangle + 3\beta_2 z^2\psi + 3\beta_2 z\psi^2 - 3\beta_2 z\langle\psi^2\rangle + \beta_2\psi^3 - \beta_2\langle\psi^3\rangle + r[-\beta\psi + \beta\langle\psi\rangle + 2\beta_1 z\psi - 2\beta_1 z\langle\psi\rangle + \beta_1\psi^2 - \beta_1\langle\psi^2\rangle + 3\beta_2 z^2\psi - 3\beta_2 z^2\langle\psi\rangle + 3\beta_2 z\psi^2 - 3\beta_2 z\langle\psi^2\rangle + \beta_2\psi^3 - \beta_2\langle\psi^3\rangle]\cos\Omega\tau = -r\left[\frac{3}{2}\beta - \beta z + \beta_1 z^2 + \beta_2 z^3\right]\cos\Omega\tau \tag{24}$$

Using the inertial approximation [7], the fast dynamic ψ is written as

$$\psi = \frac{r}{\Omega^2}\left(\frac{2}{3}\beta - \beta z + \beta_1 z^2 + \beta_2 z^3\right)\cos\Omega\tau \tag{25}$$

Inserting ψ from (25) into (23), using that $\langle cos^2 T_0\rangle = 1/2$, and neglecting terms of orders greater than three in z, give the main equation governing the slow dynamic of the motion (6).

The parameters $\omega_1^2, \rho_1, \rho_2$ and H are given, respectively, by

$$\omega_1^2 = \varpi^2 + \frac{2\beta^2 r^2}{3\Omega^2} - \frac{5\beta^3 r^2}{36\Omega^4} - \frac{\beta^4 r^4}{48\Omega^6} \tag{26}$$

$$\rho_1 = \frac{\beta}{4} - \frac{\beta^2 r^2}{3\Omega^2} + \frac{\beta^3 r^2}{12\Omega^4} + \frac{7\beta^4 r^4}{192\Omega^6} \tag{27}$$

$$\rho_2 = \frac{\beta}{24} - \frac{\beta^2 r^2}{48\Omega^2} + \frac{\beta^3 r^2}{36\Omega^4} - \frac{35\beta^4 r^4}{1152\Omega^6} \tag{28}$$

$$H = -\frac{\beta^2 r^2}{3\Omega^2} + \frac{\beta^3 r^2}{18\Omega^4} + \frac{\beta^4 r^4}{216\Omega^6} \tag{29}$$

References

[1] Binnig G, Quate F, Gerber C. Atomic force microscope. Phys Rev Lett 1986;56:930–3.
[2] Sabot J, Krempf P, Janolin C. Nonlinear vibrations of a sphere plane contact excited by a normal load. J Sound Vib 1998;214:359–75.
[3] Perret-Liaudet J, Rigaud E. Experiments and numerical results on non-linear vibrations of an impacting Hertzian contact. Part 1: harmonic excitation. J Sound Vib 2003;265:289–307.
[4] Perret-Liaudet J, Rigaud E. Response of an impacting Hertzian contact to an order-2 subharmonic excitation: theory and experiments. J Sound Vib 2006;296:319–33.
[5] Bichri A, Belhaq M, Perret-Liaudet J. Control of vibroimpact dynamics of a single-sided Hertzian contact forced oscillator. Nonlinear Dyn 2010;63:51–60.
[6] Bichri A, Belhaq M. Control of a forced impacting Hertzien contact oscillator near-subharmonic and superharmonic of order 2. Comput Nonlinear Dyn 2011;7:011003.
[7] Blekhman II. Vibrational mechanics-nonlinear dynamic effects, general approach, application. Singapore: World Scientific; 2000.
[8] Thomsen JJ. Vibrations and stability: advanced theory, analysis, and tools. Springer Berlin; 2003.
[9] Belhaq M, Fahsi A. Hysteresis suppression for primary and subharmonic 3:1 resonances using fast excitation. Nonlinear Dyn 2009;57:275–87.
[10] Fahsi A, Belhaq M. Effect of fast harmonic excitation on frequency-locking in a van der Pol–Mathieu–Duffing oscillator. Commun Nonlinear Sci Numer Simul 2009;14:244–53.
[11] Lakrad F, Belhaq M. Suppression of pull-in instability in MEMS using a high-frequency actuation. Commun Nonlinear Sci Numer Simul 2010;15:3640–6.
[12] Lakrad F, Belhaq M. Suppression of pull-in in a microstructure actuated by mechanical shocks and electrostatic forces. Int J Non-Linear Mech 2011;46:407–14.
[13] Turner A. Non linear vibrations of a beams with cantilever hertzien boundary conditions. J Sound Vib 2004;275:177–91.
[14] Nayfeh AH, Mook DT. Nonlinear oscillations. New York: Wiley; 1979.
[15] Nayfeh AH. Introduction to perturbation techniques. New York: Wiley; 1981.
[16] Kirrou I, Belhaq M. Frequency shift and hysteresis suppression in contact-mode AFM using contact stiffness modulation, in: MATEC Web of Conferences 2012 (1) 04003. DOI:1051/matecconf/20120104003.
[17] Santos S, Barcons V, Verdaguer A, Chiesa M. Subharmonic excitation in amplitude modulation atomic force microscopy in the presence of adsorbed water layers. J Appl Phys 2011;110:114902.
[18] Chiesa M, Gadelrab KR, Verdaguer A, Segura JJ, Barcons V, Neil H, Thomson NH, Phillips MA, Stefancich M, Sergio S. Energy dissipation in the presence of sub-harmonic excitation in dynamic atomic force microscopy. EPL 2012;99:56002.
[19] Chiesa M, Gadelrab K, Stefancich M, Armstrong P, Li G, Souier T, Thomson NH, Barcons V, Font J, Verdaguer A, Phillips MA, Santos S. Investigation of nanoscale interactions by means of subharmonic excitation. J Phys Chem Lett 2012;3:2125–9.
[20] Burnham NA, Kulik AJ, Gremaud G. Nanosubharmonics: the dynamics of small nonlinear contacts. Phys Rev Lett 1995;74:5092–5.

[21] Abdel-Rahman EM, Nayfeh AH. Contact force identification using the subharmonic resonance of a contact-mode atomic force microscopy. Nanotechnology 2005;16:199–207.
[22] Raman A, Melche J, Tuang R. Cantiliver dynamics in atomic force microscopy. Nanotoday 2008;3:20–7.
[23] Rabe U, Turner J, Arnold W. Analysis of the high-frequency response of atmic force microscope cantilevers. Appl Phys 1998;66:277–82.
[24] Johnson KL. Contact mechanics. Cambridge: Cambridge University Press; 1979.
[25] Rabe U, Janser K, Arnold W. Vibration of free and surface coupled atomic force microscopy cantilevers: theory and experiment. Rev Sci Instrum 1996;67:3281–93.
[26] Rabe U, Kester E, Arnold W. Probing linear and nonlinear tip-sample interaction forces by atomic force acoustic microscopy. Surf Interface Anal 1999;27:386–91.
[27] Yamanaka K, Noguchi A, Tsuji T, Koike T, Goto T. Quantitative material characterization by ultrasonic AFM. Surf Interface Anal 1999;27:600–6.
[28] Rabe U, Kopycinska-Müller M, Reinstädtler M, Hirsekorn S, Arnold W. Nonlinear effects in ultrasonic transmission in atomic force microscope contacts. In: Rudenko O, Sapozhnikov OA, editors. Proceedings of the international symposium nonlinear Acoustics Moscow, Faculty of Physics, Moscow State University, 2002;2:711–718.
[29] Rabe U, Amelio S, Kopycinska M, Hirsekorn S, Kempf M, Göken M, Arnold W. Imaging and measurement of local mechanical material properties by atomic force acoustic microscopy. Surf Interface Anal 2002;33:65–70.